Bacterial S-Layer Protein Coupling to Lipids: X-Ray Reflectivity and Grazing Incidence Diffraction Studies

Markus Weygand,* Barbara Wetzer,# Dietmar Pum,# Uwe B. Sleytr,# Nicolas Cuvillier,§ Kristian Kjaer,¶ Paul B. Howes,¶ and Mathias Lösche*

*Leipzig University, Institute of Experimental Physics I, D-04103 Leipzig, Germany; #University for Agricultural Sciences, Center for Ultrastructure Research and Ludwig-Boltzmann-Institute for Molecular Nanotechnology, A-1180 Vienna, Austria; §Institute Curie, Laboratoire de Physico-Chemie des Surfaces et Interfaces, F-75 231 Paris, France; and ¶Risø National Laboratory, Department of Solid State Physics and Chemistry, DK-4000 Roskilde, Denmark

ABSTRACT The coupling of bacterial surface (S)-layer proteins to lipid membranes is studied in molecular detail for proteins from *Bacillus sphaericus* CCM2177 and *B. coagulans* E38–66 recrystallized at dipalmitoylphosphatidylethanolamine (DPPE) monolayers on aqueous buffer. A comparison of the monolayer structure before and after protein recrystallization shows minimal reorganization of the lipid chains. By contrast, the lipid headgroups show major rearrangements. For the *B. sphaericus* CCM2177 protein underneath DPPE monolayers, x-ray reflectivity data suggest that amino acid side chains intercalate the lipid headgroups at least to the phosphate moieties, and probably further beyond. The number of electrons in the headgroup region increases by more than four per lipid. Analysis of the changes of the deduced electron density profiles in terms of a molecular interpretation shows that the phosphatidylethanolamine headgroups must reorient toward the surface normal to accommodate such changes. In terms of the protein structure (which is as yet unknown in three dimensions), the electron density profile reveals a thickness $l_z \approx 90$ Å of the recrystallized S-layer and shows water-filled cavities near its center. The protein volume fraction reaches maxima of >60% in two horizontal sections of the S-layer, close to the lipid monolayer and close to the free subphase. In between it drops to ~20%. Four S-layer protein monomers are located within the unit cell of a square lattice with a spacing of ~131 Å.

INTRODUCTION

Bacterial and archaeal surface layers are proteinaceous structures observed on the outer cell envelopes of a large number of prokaryotic organisms (for a recent compilation, see Sleytr et al., 1996a). They constitute the outermost component on such cells and consist of monomolecular crystalline protein layers that have been intensively studied for more than a decade. This research has been stimulated by both biochemical and biotechnological motivations; surface (S)-layer lattices are interesting objects with respect to their physico-chemical properties and at the same time have been demonstrated to open up new perspectives for a number of advanced applications (Sleytr and Sára, 1997; Sleytr, 1997). Recrystallized S-layers and S-layer-supported lipid films can cover holes or porous supports with apertures up to several microns in diameter and still maintain their structural integrity (Pum and Sleytr, 1994, 1996; Schuster et al., 1998a,b). The molecular details of protein coupling to lipid membranes is a particular aspect in the focus of this work.

Most S-layers studied to date consist of one single protein or glycoprotein species, which is specific for a particular bacterial or archaeal species. Structural properties of S-layers formed by different organisms, such as the degree of glycosylation or the lattice symmetry, may thus vary greatly. Molecular masses of the constituent proteins may range from ~40 to ~200 kDa (Messner and Sleytr, 1992; Sleytr et al., 1996a), lattice constants may range from 3 to 30 nm, and the S-layer thickness may range from 5 to 15 nm. On the other hand, general features are similar for many of the lattices studied so far. Within the two-dimensional (2D) crystalline unit cell, protein occupies only a fraction, typically 30–70%, of the area; this leads to the formation of well defined and identical pores. Similarly, a pronounced asymmetry of the topographical and physico-chemical properties of the two faces oriented toward and away from the cell membrane has been observed as a common feature of most S-layer lattices studied so far. The inner face, pointing to the cell membrane, is generally more corrugated than the outer face (Baumeister and Engelhardt, 1987; Hovmöller et al., 1988; Beveridge, 1994). In S-layers of bacillaceae, the outer face does not bear excess charges at physiological pH values, whereas the inner face is often net negatively charged (Sára and Sleytr, 1996). Recently it has been reported that some organisms form complex S-layer lattices consisting of different protein species (Messner and Sleytr, 1992), and it has also been shown that, depending on growth conditions, single strains may express different S-layer proteins that may form different lattices (Sára et al., 1996). It is

Received for publication 12 February 1998 and in final form 9 October 1998.

Address reprint requests to Dr. Mathias Losche, Leipzig University, Institute of Experimental Physics I, Linnestrasse 5, D-04103 Leipzig, Germany. Tel.: 49-341-9732470; Fax: 49-341-9732479; E-mail: loesche@physik.uni-leipzig.de.

B. Wetzer's current address: Rhône-Poulene Rorer, 13, Quai Jules Guesde, F-94403 Vitry sur Seine, France.

N. Cuvillier's current address: CRPP, Avenue A. Schweitzer, F-33600 Pessac, France.

P. B. Howes' current address: University of Leicester, Dept. of Physics & Astronomy, University Road, Leicester LE1 7RH, England.

0006-3495/99/01/458/11 $2.00

thus clear that S-layers are nonconserved structures of limited taxonomical value. Gene or protein sequencing, on the other hand, has shown that S-layer proteins from different organisms show a similar overall composition with a high abundance of glutamic and aspartic acid residues and little or no cysteine and methionine (Messner, 1996). Generally, S-layer lattices are self-assembled structures formed from their constituent monomeric units at their supporting envelope layer through noncovalent bonds. In Gram-positive bacteria, S-layers are associated with the peptidoglycan-containing layer, in Gram-negative bacteria with components of the outer membrane, and in most archaea with the cytoplasmatic membrane (Sleytr et al., 1996b).

A general feature of isolated S-layer proteins from bacillaceae is their ability to recrystallize at a variety of interfaces and surfaces. Reconstitution of S-layer lattices has been reported at technical surfaces such as glass, quartz, Si, Pt, or Au (Pum and Sleytr, 1996), where their structure may be characterized with high resolution using atomic force microscopy (AFM). Recrystallization has also been achieved on various artificial membrane interfaces, such as vesicles (Küpcü et al., 1995) or lipid monolayers at the surface of aqueous buffer (Pum et al., 1993; Wetzer et al., 1997). A systematic study of the association of S-layer proteins with lipid monolayers of various compositions, pH values, and ionic strengths of the buffer has recently been reported (Wetzer et al., 1998).

Although the in-plane structure of reconstituted S-layer lattices has recently been characterized with AFM in high resolution (Pum and Sleytr, 1995), the classical method of structural characterization is transmission electron microscopy (TEM), which is capable of imaging the lattices as formed in vivo, after freeze-etching, or upon reconstitution on various interfaces, after heavy ion staining (Pum et al., 1989). Unfortunately, neither characterization technique reveals any information on the spatial relation of the lipid and the protein components of the composite lipid/protein layer, and only TEM is capable of providing some limited information on the density distribution perpendicular to the interface normal (Amos et al., 1982). We have therefore recently started to characterize the formation of reconstituted S-layer lattices at lipid surface monolayers with alternative methods. Particularly revealing was a dual-label fluorescence microscopy study in which we have investigated the complicated interrelation between order and disorder in both the lipid and protein components on the mesoscopic (micrometer) length scale (Diederich et al., 1996). We found that the local order of the aliphatic chains in the surface monolayer controls the nucleation and growth of 2D S-layer protein crystallites, whereas Fourier transform infrared (FTIR) spectroscopy indicated that protein crystallization in turn increases the order of the aliphatic chains. It was concluded that the order on the lipid chains and in the protein aggregates is mutually dependent. From an analysis of the temporal development of protein adsorption and 2D crystal nucleation and growth we derived indirect arguments that the coupling of the protein to the lipid might occur via the lipid headgroups, implying that direct contacts between the protein and the hydrophobic sections of the lipid monolayer are improbable. In this work, we have followed up these observations and have collected direct experimental evidence on the microscopic, i.e., molecular, details of protein/lipid coupling using x-ray reflectometry. We have further utilized grazing incidence x-ray diffraction (GIXD) at the buffer/air interface to study the rearrangement of aliphatic chains in the lipid monolayer upon protein adsorption and crystallization. We have also characterized the crystallinity of the S-layer protein itself with GIXD. From these observations a detailed picture of the coupling of an S-layer protein to a phospholipid surface monolayer is developed.

MATERIALS AND METHODS

Bacillus sphaericus strain CCM2177 was obtained from the Czech Collection of Microorganisms (Brno, Czech Republic). *B. coagulans* E38–66 was from F. Hollaus (Zuckerforschung Tulln, Tulln, Austria). Growth conditions of the bacteria in continuous culture were as reported (Sleytr et al., 1986), and extraction of the S-layer protein with guanidine hydrochloride (G-HCl, 5 M in 50 mM Tris/HCl buffer, pH 7.2, 20°C) was performed as described (Sleytr et al., 1986). G-HCl extracts were dialyzed against H_2O (*B. sphaericus*) or 10 mM $CaCl_2$ (*B. coagulans*). The amino acid composition of the S-layer protein from *B. sphaericus* CCM2177, c.f. Table 1, has been determined in a standard procedure (Altmann, 1992) that is incapable of quantifying proline. Also, cysteine and tryptophan are too labile for a quantification with this technique. Furthermore, neither glutamine and glutamic acid nor asparagine and aspartic acid can be discriminated with this method. Methionine and histidine were found to be below the detection limit. Cysteine is low in abundance in other S-layer proteins for which the amino acid composition has been determined (Messner, 1996).

Self-assembly products were sedimented for 15 min at 40,000 × *g* and 4°C immediately before using the protein solution in experiments. The clear supernatant that contains the disassembled S-layer protein monomers (~2 mg/ml of the solution) was injected directly into the subphases of phospholipid monolayers in the Langmuir film balance. Dipalmitoylphos-

TABLE 1 Amino acid composition of the S-layer protein from *B. sphaericus* CCM2177 as determined using the method described by Altmann (1992)

Amino acid	Mol %	Wt %
Lysine	4.86%	6.10%
Arginine	1.12%	1.71%
Histidine	~0	~0
Asparagine/aspartic acid	14.99%	16.63%
Cysteine	ND	ND
Threonine	12.59%	12.38%
Serine	5.74%	4.86%
Glutamine/glutamic acid	12.01%	14.96%
Proline	ND	ND
Glycine	8.98%	4.98%
Alanine	14.99%	10.36%
Valine	9.80%	9.44%
Isoleucine	3.35%	3.69%
Leucine	5.99%	6.58%
Methionine	~0	~0
Tyrosine	2.16%	3.43%
Phenylalanine	3.41%	4.89%
Tryptophan	ND	ND

phatidylethanolamine (DPPE) was purchased from Avanti Polar Lipids (Birmingham, AL) and used as received. It was dissolved in $CHCl_3$/CH_3OH (3:1; Merck, Darmstadt, Germany, p.a. grade) to form a spreading solution of ~1.0 mg/ml. Ultrapure H_2O was prepared by filtering in a Milli-Q (Millipore, Bedford, MA) apparatus.

X-ray specular reflection and GIXD experiments were performed at the BW1 beam line of HASYLAB (DESY, Hamburg, Germany). In addition, x-ray reflection measurements in a more confined momentum transfer regime from pure phospholipid monolayers as well as confirmation experiments on protein/lipid layers were conducted in collaboration with F. Rondelez at the Institute Curie (Paris, France). X-ray experiments at Hamburg were performed using a custom-built Langmuir film balance (surface area, 16×30 cm^2) incorporated in a gas-tight, thermostatted Al container with Kapton windows for the x-ray beam (Lösche et al., 1993). A polished (λ/10) Pyrex (boron silicate) glass block, inserted into the subphase to diminish to ~300 μm, the depth under the beam footprint on the monolayer was used to suppress surface waves in the film balance. The film balances were operated under computer control (R&K, Mainz, Germany).

Experiments were performed at room temperature ($T = 21 \pm 1$°C). Lipid films were prepared by spreading DPPE from the stock solution on a buffer containing 10 mM $CaCl_2$, buffered with ~1 mM boric acid to pH 9.0 (*B. sphaericus*) or unbuffered, pH ~6 (*B. coagulans*). After evaporation of the solvent, the films were compressed to a surface pressure π of typically 28 mN/m. To reduce the volume of the subphase, a clean glass rod with square cross section was then inserted behind the barrier. This glass rod divided the subphase into a smaller portion, supporting the interface film and containing the barrier, and a larger portion with the clean surface, such that the volume accessible to perfusion with the protein was reduced from ~300 ml to ~70 ml. After optionally characterizing the phospholipid surface layer, typically 5–10 ml of the S-layer protein solution was injected through the compressed lipid monolayer into the aqueous subphase. The protein was allowed to incubate the compressed phospholipid monolayer for 10–12 h, and progress of the film formation was sometimes monitored by recording the reflectivity at constant momentum transfer Q_z. In such cases, protein film formation, or reorganization within the protein film, was assumed to be completed when no change in the reflectivity signal was observed for more than 30 min. The propensity of the S-layer protein to crystallize under the DPPE monolayer was very sensitive to mechanical vibrations; disturbances of the sample film during protein adsorption inhibited protein crystallization.

The set-up at the undulator beamline BW1 has been described in detail (Weissbuch et al., 1997). The x-ray wavelengths, chosen in different runs, were between $\lambda = 1.38$ and 1.45 Å. Experiments were performed with a wet He atmosphere over the sample films. The beam footprint on the sample was $\sim 5 \times 50$ mm^2 in reflectivity experiments and in GIXD experiments at large horizontal scattering angles, $2\theta_{xy}$, i.e., when diffraction from the lipid chains was observed. It was narrowed down by an additional pair of horizontal slits to a size of $\sim 1 \times 50$ mm^2 at low $2\theta_{xy}$ (~1°), i.e., when diffraction from the surface bound protein was observed, to eliminate background scattering from the Kapton windows. For reflectivity measurements, the incident beam was attenuated using various calibrated Al absorbers in different regimes of Q_z. At $Q_z > 0.4$ Å^{-1}, the full (nonattenuated) beam was used in the experiments. Whereas in GIXD experiments with lipid monolayers beam damage is usually a minor problem only, we observed that it does pose a significant problem when protein/lipid films are illuminated with the full x-ray beam. In separate experiments we have measured the temporal decay of low-index Bragg reflections in the full beam and in the GIXD measurements we have translated the sample laterally such that new sample film was continuously moved into the beam footprint. This ensured that at any time of the diffraction experiments largely undamaged film was illuminated.

After completing the in situ x-ray scattering experiments, the crystallinity and the completeness of the reconstituted protein lattice was routinely checked by transferring the lipid/protein sample films to electron microscope (EM) grids coated with carbon films. Typically, 15–20 EM grids were placed at different locations on the film balance in the region of the beam footprint. They were inspected in the EM (Philips CM12) after fixation with glutaraldehyde and negative staining with uranyl acetate.

Reflectivity data were analyzed with two different strategies; cf. Figs. 1 and 2. First, using conventional slab models (Als-Nielsen and Kjaer, 1989; Als-Nielsen and Möhwald, 1991; Als-Nielsen et al., 1994; Vaknin et al., 1991), i.e., by optimization of parameterized layered scattering length

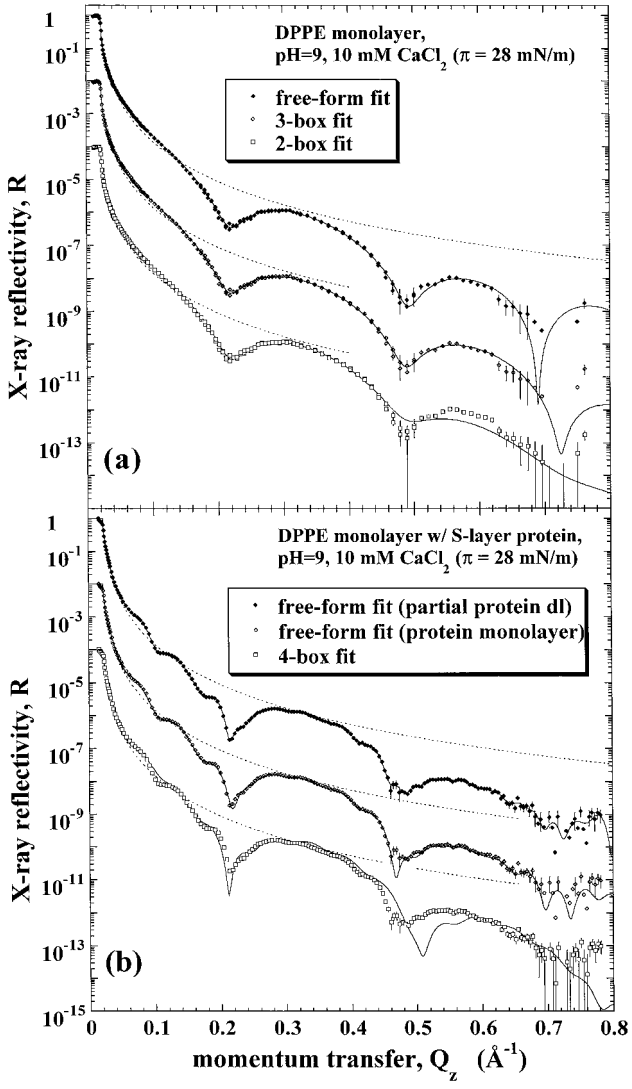

FIGURE 1 X-ray reflectivities of a DPPE monolayer on aqueous subphase (10 mM $CaCl_2$, pH 9) at a surface pressure $\pi = 28$ mN/m (*a*) and the same monolayer after adsorption and recrystallization of an S-layer from *B. sphaericus* CCM2177 protein (*b*). The surface pressure has risen to ~35 mN/m during S-layer formation. Results from various fit strategies, as described in the text and indicated in the panels, are shown. They are displaced for clarity and compared with identical data sets within each panel. Error bars are given on all data points, except for a few at high Q_z where they are omitted in the upper two curves for clarity; in most cases, they are smaller than the printed symbols. The term free-form fit in the legends relates to the model-independent inversions of the experimental results based on b-splines as described in the text. The term partial protein dl relates to a model in which it was assumed that underneath the recrystallized primary S-layer a partial (~30% density of the S-layer) second layer has been formed in which the protein is bound with its reverse side attached to the S-layer; cf. footnote in the main text.

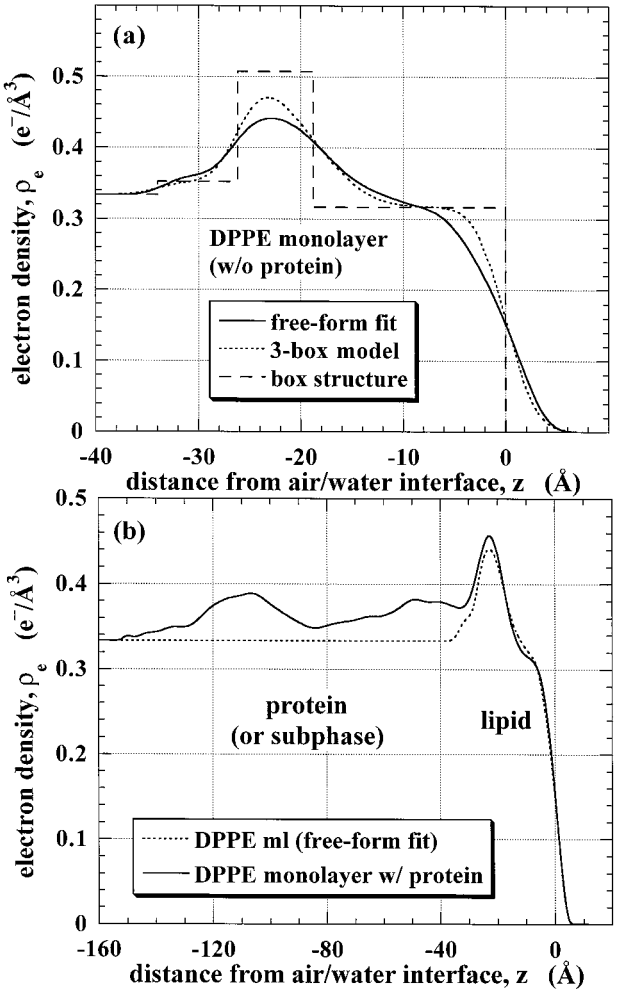

FIGURE 2 Electron density profiles $\rho_e(z)$ used to model the experimental data shown in Fig. 1. (*a*) DPPE monolayer (10 mM $CaCl_2$, pH 9) at π = 28 mN/m. Two modeling strategies have been used (see text) that both describe the experimental data satisfactorily. A model-independent inversion based on b-splines (——) leads to the reflectivity shown in the upper curve in Fig. 1 *a*. The middle curve in Fig. 1 *a* has been constructed using a three-box model (- - -) with the parameters d_{chain} = 18.8 Å, ρ_e^{chain} = 0.317 $e^-/Å^3$; d_{head} = 7.4 Å, ρ_e^{head} = 0.507 $e^-/Å^3$; d_{ul} = 7.8 Å, ρ_e^{ul} = 0.352 $e^-/Å^3$; $\sigma_{air/chain}$ = 3.2 Å, $\sigma_{chain/head}$ = 5.8 Å, $\sigma_{head/ul} = \sigma_{ul/subphase}$ = 2.7 Å, where the underlayer (ul) underneath the lipid headgroups is believed to contain Ca^{2+} cations (see text). The structure of the box model (i.e., the layers with $\sigma_i = 0$) is indicated as a dashed line. (*b*) Comparison of $\rho_e(z)$ of the surface layer structure before (- - -) and after (——) S-layer protein (*B. sphaericus* CCM2177) adsorption to the DPPE monolayer. The electron density profile shown as a solid line has been used to construct the reflectivity shown in the middle curve in Fig. 1 *a*.

density (SLD) distributions of the form:

$$\rho(z) = \sum_{i=0}^{n} \frac{1}{2}(\rho_{i+1} - \rho_i) \times \left(1 - \mathrm{erf}\left(\frac{z - z_i}{\sqrt{2}\sigma_i}\right)\right), \qquad (1)$$

where ρ denotes the SLD and ρ_i is the (homogeneous) SLD in layer i (i = 0 points to the air space and $i = n + 1$ points to the aqueous substrate), z denotes the distance from the surface, and z_i are the locations where the SLD values change from ρ_i to ρ_{i+1}. σ_i represents the r.m.s. roughness values of the interfaces between adjacent layers, which are described as error functions (erf). Second, using the model-free constrained least-squares approach of Skov Pedersen and Hamley (Hamley and Skov Pedersen, 1994; Skov Pedersen and Hamley, 1994b), which uses b-splines $B_i(z)$ to describe the SLD distribution across the surface:

$$\rho(z) = \sum_{i=1}^{N} a_i B_i(z), \qquad (2)$$

where N is determined by the accessible Q_z range via the sampling theorem. In this approach, $\rho(z)$ is determined in a constrained least-squares fit which aims at suppressing solutions with large oscillations in $\rho(z)$ that often represent unphysical situations. Details are described in Skov Pedersen and Hamley, 1994a,b.

Diffraction from 2D crystalline patches yields intensity, which, as a function of the horizontal component, $Q_{xy} \approx (4\pi/\lambda)\sin(2\theta_{xy}/2)$, of the scattering vector, peaks at Bragg positions Q_{xy}^{hk}. In the absence of a crystalline repeat in the vertical (z) direction, the intensity extends as a smooth function, the Bragg rod profile $I_{hk}(Q_z)$ of the vertical component of the scattering vector, $Q_z \approx (2\pi/\lambda)\sin(\alpha_f)$, where α_f is the vertical direction of the scattered rays. The Bragg rod profiles resulting from the phospholipid chains may be modeled (Als-Nielsen and Kjaer, 1989; Als-Nielsen et al., 1994) by

$$I_{hk}(Q_z) = \sum_{(hk)} |V(\alpha_f)|^2 \times \mathrm{sinc}^2\left[\frac{1}{2}L(Q_z \cos\vartheta - (\mathbf{Q}_{xy}^{hk} \cdot \hat{\mathbf{e}})\sin\vartheta)\right] \times \exp(-Q_z^2\sigma^2), \qquad (3)$$

where $|V|^2$ is the Yoneda-Vineyard peak (Vineyard, 1982), L is the length of the palmitoyl chains, $\hat{\boldsymbol{e}}$ is a horizontal unit vector defining the tilt azimuth, $\boldsymbol{Q}_{xy}^{hk}$ is the in-plane reciprocal lattice vector, σ is the vertical r.m.s. displacement, and the sum is over all Bragg reflections contributing to the intensity at the position Q_{xy}^{hk}. From Eq. 3 it follows (Kjaer, 1994) that for each peak (h,k) the coordinates $\boldsymbol{Q}_{xy}^{hk}$ and Q_z^{hk} are related by

$$Q_z^{hk} = (\mathbf{Q}_{xy}^{hk} \cdot \hat{\mathbf{e}})\tan\vartheta, \qquad (4)$$

where ϑ is the tilt angle of the chains measured from the surface normal. For well resolved peaks, the ϑ and the azimuthal direction $\hat{\boldsymbol{e}}$ can be deduced directly from the set of equations, Eq. 4.

RESULTS

We have measured the x-ray reflectivity of DPPE on 10 mM $CaCl_2$ at pH 9.0 before and after adsorption and crystallization of S-layer protein from *B. sphaericus* CCM 2177. Pure phospholipid monolayers were characterized on the liquid surface reflectometer at the Institute Curie and occasionally on BW1, where the accessible Q_z range extends to almost 0.8 $Å^{-1}$. As in the case of x-ray reflectivity from dipalmitoylphosphatidylcholine monolayers on pure water subphases, the data, shown in Fig. 1 *a*, were initially interpreted in terms of a layer model (Helm et al., 1987; Vaknin et al., 1991), Eq. 1. Subsequently, to afford a direct comparison with the situation after S-layer formation at the monolayer, the same data were also analyzed in the model-free approach of Skov Pedersen and Hamley. Although this latter approach does not directly lead to a molecular interpretation of the interface structure, it is well suited to generate electron density profiles that give rise to reflectivity models that describe the experimental data with high fidelity; cf. Fig. 1 *a*. Cross-reference to the layer models

then enables the choice of a physically reasonable solution from the model-free approach, in cases where ambiguities occur, as well as a discussion of the result in terms of a molecular structure.

The reflectivity from floating phospholipid monolayers on aqueous subphases have traditionally been interpreted in terms of two-layer models (Helm et al., 1987; Vaknin et al., 1991) in which one layer contains the hydrophobic chains and one layer contains the hydrated lipid headgroups. Most of the data analyzed in earlier investigations, however, reached only $Q_z \approx 0.4-0.5$ Å^{-1} (or even considerably lower Q_z values in the case of neutron reflectometry work). In this work, we have determined the x-ray reflectivities of phospholipid monolayers and protein/phospholipid layer systems at Q_z values as large as 0.8 Å^{-1}. Data analysis revealed that although a conventional two-layer model was capable of describing the experimental data sufficiently well up to $Q_z \approx 0.4$ Å^{-1} it failed at higher momentum transfer (lower curve in Fig. 1 *a*). On the other hand, we were able to describe the extended data set satisfactorily with a three-layer model in which the roughness parameters σ_i were individually adjusted (middle curve in Fig. 1 *a*). The free-form fit (upper curve in Fig. 1 *a*) describes the experimental data equally well. In Fig. 2 *a*, the electron density profile derived from the three-layer model (dashed lines) describing a DPPE monolayer on 10 mM $CaCl_2$ is compared with the electron density derived from the model-free approach (solid line). It is obvious that the features of the three-layer model are generally consistent with the result from the model-free approach. The layer closest to the air space contains the densely packed hydrophobic chains ($\rho_e \approx 0.318$ e$^-$/Å^3) and has a thickness $d_{chain} \approx 19$ Å. The headgroups are organized in an adjacent layer, closer to the aqueous subphase, which has a thickness of $d_{head} \approx 7.4$ Å and includes on average ~1.2 water molecules per PE incorporated in the headgroups. This is consistent with an orientation of the dipole connecting the phosphate and amine moieties being almost parallel to the interface. In comparison with the conventional interpretation of the molecular structure of phospholipid monolayers in terms of two-layer models, the interface between the lipid's headgroups and its hydrocarbon chains is unexpectedly broad, $\sigma_2 \approx 5.8$ Å, which is significantly larger than the value $\sigma \approx 3$ Å usually attributed to thermally excited capillary waves on the subphase and applied to all interfaces between different slabs describing a lipid monolayer. Moreover, the peak electron density in the headgroup is considerably lower and the headgroup further extended along the surface normal than in the results from a traditional two-slab description. In addition, there is a pronounced accumulation of electron density below the phospholipid headgroup, in the range -34 Å $< z < -26$ Å, counting from the alkane/air interface located at $z = 0$. We have first observed this contribution to the electron density profile in the model-free approach and found later that it requires involving a third slab for a satisfactory description of the experimental data beyond $Q_z \approx 0.5$ Å^{-1} in the layer model description. This contribution to the ρ_e profile might be interpreted as either an accumulation of Ca^{2+} ions in the headgroup region of the lipid or a partial ordering of water molecules in close contact with the headgroup resulting in a higher density of water immediately underneath the headgroup layer. Although the latter interpretation would only require an increase in the water density by ~5% we also note that alternatively an accumulation of ~0.3 Ca^{2+} ions per lipid molecule is sufficient to account quantitatively for the observed increase in electron density. In what follows we will use the model-free result to discuss the impact of the recrystallized S-layer on monolayer structure.

The x-ray reflectivity of the surface layer system after adsorption and recrystallization of the S-layer protein from *B. sphaericus* CCM2177 to DPPE is distinctively different from that of the lipid-only monolayer profile. Fig. 1 *b* shows a data set measured at DESY in which the reflectivity has been determined over nine orders of magnitude in a Q_z range from 0.015 to 0.8 Å^{-1}. To confirm this result, we have measured similarly prepared lipid/protein surface layers on the x-ray reflectometer at the Institute Curie in a Q_z range between 0.007 and 0.45 Å^{-1} over approximately seven orders of magnitude and found agreement between the measurements within experimental error (data not shown). TEM micrographs of lipid/protein interface layers transferred after reflectivity experiments showed complete 2D S-layer lattices composed of crystalline domains with average diameters of ~5 μm. No signs of beam damage from the x-ray exposure was detected in the electron micrographs.

For a quantitative analysis of the reflectivity data shown in Fig. 1 *b* we have again employed the two different approaches outlined above. In the layer model, Eq. 1, we have assigned two slabs to the lipid chains and headgroups and two additional slabs to the adsorbed protein layer. We found that a three-layer model (two slabs for the lipid plus one single slab to describe the protein) was completely inadequate for modeling the experimental data. By contrast, the four-slab approach affords a qualitatively correct description of the x-ray data in the low Q_z regime (<0.3 Å^{-1}, cf. lower curve in Fig. 1 *b*). The best fit of the x-ray data is found with a layer structure in which the protein is described by one slab with a lower content of protein (~35 vol%)* and a thickness of ~45 Å close to the lipid and one slab with a larger content of protein (~46 vol %) and a thickness of ~51 Å further away from the lipid, such that the total thickness of the adsorbed protein amounts to ~95 Å, consistent with data derived from AFM und TEM

* Protein volume fractions throughout this work have been determined from the data in Table 1 on the basis of the volumes determined for crystallized amino acids (Perkins, 1988), corrected for a reduction in packing density of the molecules in the protein (Lösche et al., 1993). The average electron density of the protein computed from the data in Table 1 is $\overline{\rho_e} = 0.412$ e$^-$/Å^3. Variations of the relative amounts of asparagine/aspartic acid and glutamine/glutamic acid affect this result by less than 1.3%.

(Pum et al., 1997). This model reproduces the average reflectivity and the positions of the undulations in the reflectivity curve faithfully and particularly the position of the reflectivity minimum at $Q_z \approx 0.215$ Å^{-1} is well described. The amplitudes of the undulations in the reflectivity curve, however, are not well reproduced by this model, and at larger Q_z, data and model reflectivity are in serious disagreement. The second major minimum in the reflectivity curve is predicted at $Q_z \approx 0.51$ Å^{-1} by the model, whereas it is actually observed around 0.485 Å^{-1} (lower curve in Fig. 1 *b*).

A much better description of the experimental x-ray reflectivities is afforded with the model-free approach developed by Skov Pedersen and Hamley (1994b), Eq. 2; cf. middle and upper curves in Fig. 1 *b*. Fig. 2 *b* shows ρ_e profiles of the monolayer before (dashed line) and after (solid line) protein adsorption and crystallization. An electron density profile extending from $z = 0$ to -150 Å, where it reaches the constant value attributed to the bulk aqueous subphase, models the measured data set with high fidelity (middle curve in Fig. 1 *b*), suggesting that a molecular protein sheet is attached to the lipid headgroups of the surface monolayer. Only minor discrepancies between the data and the model are observed in the Q_z regime around 0.48 Å^{-1}, the region of the second major minimum in the reflectivity, as well as at $Q_z > 0.7$ Å^{-1}, a region where the experimental error bars are already large.* The reflectivity model function derived from a partial-protein double-layer model (see footnote) is shown in the upper curve in Fig. 1 *b*.

In what follows we will discuss the structural properties of the lipid monolayer with the attached primary S-protein layer (*B. sphaericus* CCM2177) and consider the partial secondary protein layer as a contamination adhering to this structure that comes about due to the extended time span (~15 h) needed for sample preparation and measurement. Fig. 2 *b* shows that the lipid monolayer, in the region $z \approx -30$ to 0 Å, has qualitatively similar features with and without adsorbed S-layer protein. The protein layer is easily recognized at larger distances from the surface, between $z \approx -30$ and -140 Å. It is characterized by two distinct bumps in ρ_e with maxima at $z \approx -45$ and -105 Å. Between these two maxima, ρ_e drops to a minimum at $z \approx -80$ Å. Consistent with the fact that ρ_e of protein matter is considerably larger than that of H_2O (Perkins, 1988), the profile never drops below the subphase value $\rho_e = 0.334$ e$^-$/Å^3 in the region between $z = -150$ and -30 Å. The complex structural profile of the protein monolayer retrieved in this approach to data evaluation explains why a four-slab model describes the experimental data rather well whereas a three-slab model fails to do so.

Direct evidence for the formation of a 2D S-layer protein crystal layer under DPPE monolayers is obtained from the observation of GIXD. Fig. 3 shows a contour plot (intensity as a function of Q_{xy} and Q_z) of the diffraction from the *B. sphaericus* CCM2177 S-layer protein. EM and optical microscopy consistently show that the size of the 2D protein crystals is in the range of a few microns (Diederich et al., 1996). As the beam footprint on the sample film is much larger, one observes Bragg diffraction from a 2D crystal powder, and it is not possible to discriminate different diffraction peaks (h, k) if they have the same modulus $|\mathbf{Q}_{xy}^{hk}|$. Over the complete accessible Q_{xy} range up to $\{h, k\} = \{5,1\}$, the observed peak positions are consistent with a square lattice of dimensions $|\mathbf{a}| = |\mathbf{b}| = 130.5$ Å; cf. Fig. 3.

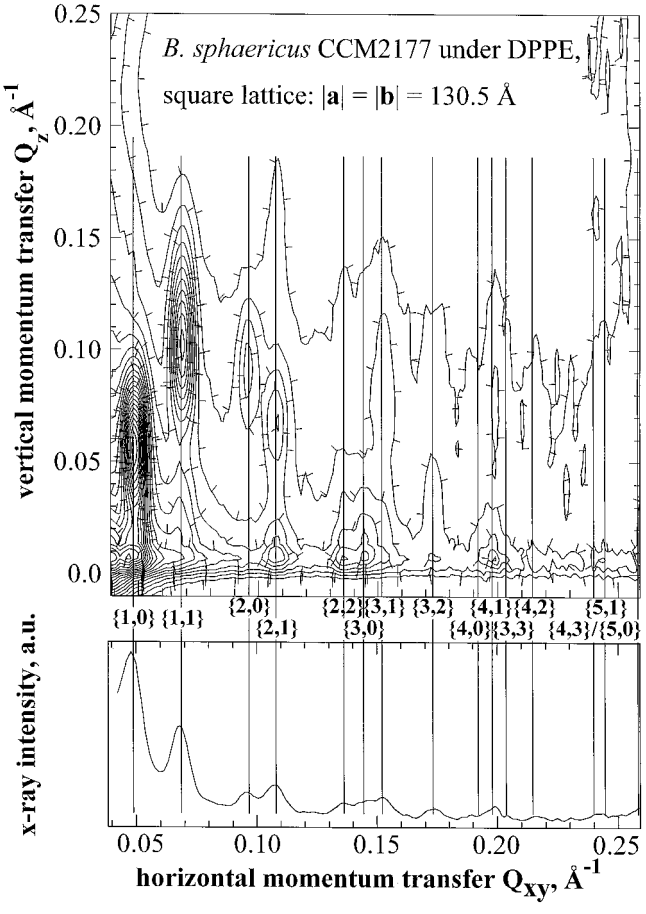

FIGURE 3 GIXD from an S-layer lattice (*B. sphaericus* CCM2177) reconstituted underneath a DPPE monolayer. (*Top*) Contour plot of the diffracted intensity $I(Q_{xy}, Q_z)$. (*Bottom*) Q_z-integrated diffraction intensity $I(Q_{xy})$. $I(Q_{xy}, Q_z)$ has been integrated between $Q_z = -0.05$ and 0.20 Å^{-1}. Also indicated are the {h, k} indices corresponding to a square lattice with $|\mathbf{a}| = |\mathbf{b}| = 130.5$ Å.

* An even better description of the experimental data is obtained if the model allows for the partial formation of a second molecular protein layer underneath the first. A b-spline model of the interface extending to $z = 240$ Å describes the data nearly perfectly and suggests that ~30% of the interface is covered with S-layer protein in a secondary layer. A comparison of the ρ_e profile in the region $z = -240$ to 140 Å and $z = -140$ to 40 Å suggests also that protein in the secondary layer is presumably attached with its reverse side to the protein in the primary layer. We note that the ρ_e profiles of the models comprising only one protein layer and the one comprising a partial secondary layer are virtually indistinguishable in the region $z = -140$ to 0 Å such that one may discuss the structural properties of the lipid surface monolayer and the protein layer immediately attached to it equally well within the frame of both models.

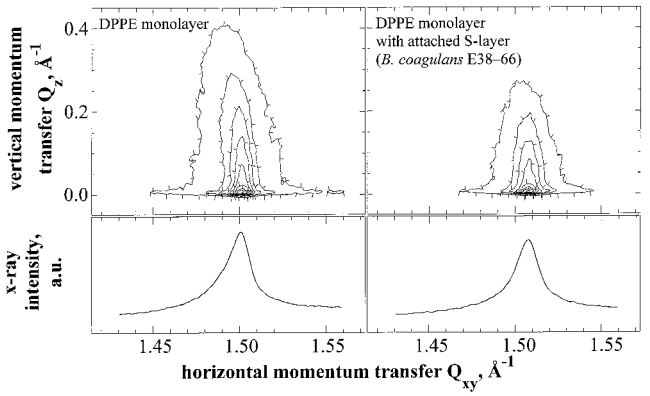

FIGURE 4 GIXD from a DPPE monolayer before ($\pi \approx 28$ mN/m) and after ($\pi \approx 35$ mN/m) adsorption and crystallization of S-layer protein from *B. coagulans* E38–66 on pure water. The surface area has been kept constant during the S-lattice formation. (*Top*) Contour plot of $I(Q_{xy}, Q_z)$. (*Bottom*) Q_z-integrated diffraction intensity $I(Q_{xy})$.

Independent of the diffraction from the 2D protein crystal, one may observe GIXD from the DPPE monolayer. Fig. 4 shows in contour plots the diffraction intensity of the first-order peaks of the hexagonal phase formed by the palmitoyl chains of DPPE before and after crystallization of the S-layer protein from *B. coagulans* E38–66.* It is apparent that the reorganization of the lipid chains upon crystallization of the protein at the lipid monolayer is minimal. Quantitatively, the hexagonal lattice of the alkyl chains shrinks marginally (Q_{xy} increases from ~1.508 to ~1.514 Å^{-1}) and the chains are slightly more upright at the interface, as deduced from the Bragg rod, which extends less into Q_z after protein adsorption. This observation excludes the possibility that the protein infers any major reorganization of the lipid monolayer, as far the lipid chains are concerned.

DISCUSSION

The recrystallization of S-layer proteins at lipid interfaces poses intriguing questions regarding the interaction between the constituents of the system that bear important implications for its structure and dynamics. We have started to address these issues in earlier investigations (Diederich et al., 1996); they are the focus of related work, in which we have systematically studied the propensity of the S-layer protein from *B. coagulans* E38–66 to recrystallize underneath monolayers of various lipids, distinguished by the degree of saturation and the lengths of their hydrophobic chains and the size, polarity, and charge of their headgroups, under various subphase constitutions with respect to pH and ionic strength (Wetzer et al., 1998). A sensible model for the reconstitution of S-layers at lipid interfaces must account for the experimental observation that the protein is preferentially adsorbed to the fluid lipid phase, whereas crystallization is much faster underneath the ordered hexatic phase. At the same time, protein recrystallization at disordered lipid phase areas increases the order of the lipid chains there (Diederich et al., 1996).

Electrostatic interactions play a prominent role in the coupling and crystallization of the proteins at lipid monolayers (Wetzer et al., 1998); the exposure of cationic charges by the lipid headgroups is required for the formation of reconstituted S-layers from *B. coagulans*, and it seems of minor importance whether these exposed charges are the trimethylamine functions in the zwitterionic choline headgroup, Ca^{2+} ions bound to zwitterionic or negatively charged headgroups, or positively charged headgroups, such as trimethylammonium propane. From these observations it appears that specific contacts of positive charges with negative charges exposed by anionic side chains of the proteins are required for protein adsorption and crystallization. Interestingly, S-layer protein crystallization occurs at choline headgroups in pure H_2O whereas it has not been observed at ethanolamine headgroups on that subphase. This is consistent with the finding that the anionic groups on the protein are located in shallow pockets at the surface facing the lipid membrane (Sára and Sleytr, 1993, 1996), such that the charges are accessible only to moieties that protrude somewhat from the interface by means of a short tether.

In an S-layer, a large number of lipid headgroups face each protein in the crystal lattice. For example, in the S-layer formed by *B. sphaericus* CCM2177, ~100 lipids occur per protein, or ~400 per unit cell of the S-lattice. Undoubtedly, only a small fraction of those lipids are coupled to the protein in specific electrostatic contacts. From this conception, the speculation arises that some of the lipids bound to the crystalline S-layer are immobilized whereas others, presumably the largest fraction, are more mobile as their headgroups are not specifically attached to the S-layer. We expect thus that some of the lipids bound to the S-lattice show a lateral mobility significantly reduced below that of the remaining fraction and have coined the term semifluid membrane to describe this property of the attached lipid layer (Pum and Sleytr, 1994).

Molecular details in the coupling of S-layers (*B. sphaericus* CCM2177) to phospholipid monolayers is the focus of the study reported here. Such S-layers are formed from one single nonglycosylated protein species with a molecular weight $M_r \approx 120{,}000$ (Pum and Sleytr, 1994). A square lattice with a lattice constant $|\mathbf{a}| = 128$ Å has been observed in electron microscopy of the uranyl-stained S-layer (Pum and Sleytr, 1994) and in scanning force microscopy (Pum et al., 1997; Wetzer et al., 1997). The best estimate to date of the thickness l_z of the S-layer derives from AFM height measurements at the edge of incompletely recrystallized lattices and shows $l_z \approx 80$ Å. A quantitative evaluation of the results presented in the preceding section leads to a

* We have also observed the GIXD from DPPE before and after adsorption of the S-layer protein from *B. sphaericus* CCM2177 at pH 9.0. The results are similar to those in Fig. 4 and show only minor structural differences in the lipid chain regions due to the protein recrystallization. However, for technical reasons we have never managed to measure both data sets on one lipid monolayer, before and after protein recrystallization.

detailed conception of the coupling of the S-layer to lipid membranes and the structural rearrangements that the protein infers in phospholipid monolayers.

For the S-layer protein from *B. coagulans* E38–66, GIXD from the lipid chains before and after protein adsorption shows (Fig. 4) that rearrangements in the hydrophobic part of the monolayer are small. This is surprising in view of a significant increase in surface pressure that is typically observed upon S-layer protein incubation of phospholipid monolayers (Diederich et al., 1996). In quantitative terms we find that the lattice constant decreases by ~0.35% from 4.183 to 4.168 Å; i.e., the area occupied by the chains and thus the molecular density of DPPE in the surface monolayer decreases by less than 1%. This small area reduction is accompanied by a slight decrease of the chain tilt angle from $\vartheta \approx 9.5°$ to ~6°. These results provide definite evidence that the protein does not interpenetrate the hydrophobic section of the lipid monolayer, a conjecture that was drawn from indirect evidence obtained in earlier fluorescence microscopic work (Diederich et al., 1996).

This conclusion is also supported by a comparison of the ρ_e profiles in the region of the DPPE monolayer before and after S-layer recrystallization (Fig. 5). The profiles are essentially identical in the region of the hydrophobic chains (as assigned in the layer model). The integrated electron densities differ by less than 0.15%, which is well below the precision of the technique. By contrast, the electron density after S-layer formation is slightly but significantly larger in the headgroup region of the lipid. This is very likely due to partial insertion of protein, presumably amino acid side chains, into the lipid headgroup region. The integrated electron density difference in the space occupied by one headgroup before and after S-layer formation (cross-hatched area in Fig. 5) amounts to ~4.31 electrons. If one assumes that this change is due to amino acid side chains replacing water molecules associated with the lipid's headgroups, it must be noted that this is more than the ~1.2 H_2O molecules that we have quantified to be interdispersed between the headgroups before protein incubation (see above).* Consequently, the increase in electron density observed in this region can be quantitatively accounted for only if one assumes that the lipid headgroups, which are oriented essentially parallel to the interface in the unperturbed monolayer (Pink et al., 1997), reorient somewhat during protein adsorption toward the surface normal. This is also consistent with the finding that the increase in electron density affects the entire headgroup. In particular, an increase of ρ_e is observed at the phosphate moiety (the region where the ρ_e profile reaches its maximum) and even ~4 Å above where the glycerol backbone is located; if the peptide inserts that deeply into the monolayer, the lipid's headgroups must reorient to accommodate the amino acid side chains.

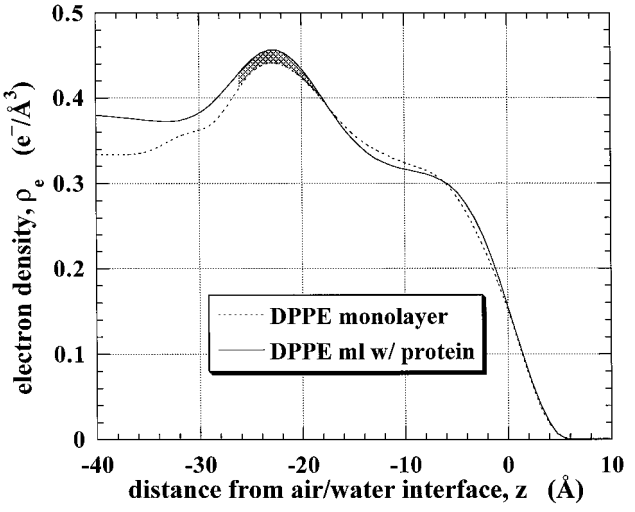

FIGURE 5 Details of the ρ_e profiles in the region of the DPPE monolayer before (- - -) and after (——) S-layer formation (*B. sphaericus* CCM2177). The data are the same as those shown in Fig. 2 *b*. The cross-hatched area, indicating the increase in scattering length of the PE headgroup, amounts to more than four electrons and is consistent with the replacement of ~1.5 H_2O molecules per lipid by peptide material upon protein adsorption to the monolayer.

A schematic representation of the surface topography as derived from reflectivity measurements is depicted in Fig. 6. To accommodate amino acid side chains that interpenetrate the lipid's headgroups upon S-layer protein binding, the orientation of PE headgroup is tilted more toward the surface normal at least on some of the lipids in the monolayer that are directly associated with the peptide. This is likely to facilitate an enhancement of electrostatic interactions between the amine functions of the lipid and anionic amino acid side groups, which are presumably buried in pockets on the protein's surface (Sára and Sleytr, 1996). Within the precision of the experiment one cannot, however, determine whether all PE headgroups reorient by a relatively small angle or a small number of headgroups per protein unit in the S-layer reorient by a large angle. The increase in electron density within the headgroups upon peptide insertion, consistent with an interpretation that at most one amino acid side chain per three or four lipids inserts into the monolayer, leaves two possibilities open. It might well be that amino acid side chains interpenetrate the monolayer rather homogeneously, such that each side chain is in contact with a number of lipid headgroups and all headgroups are affected; alternatively, peptide might cluster within the lipid's headgroup region, such that some headgroups are strongly affected while some are not.

Information on the topography of the 2D S-layer protein crystal along the surface normal can be extracted from the

* If peptide with an average electron density $\rho_{pr} = 0.412\ e^-/Å^3$, the average value of the S-layer protein, is thought to replace H_2O with a bulk density $\rho_e^{H_2O} = 0.334\ e^-/Å^3$, an increase of 4.3 electrons in the headgroup volume amounts to a volume exchange of >50 $Å^3$, i.e., more than the water actually contained in that region before protein adsorption. With a similar approximation one may estimate that the minimal increase in headgroup layer thickness is ~1 Å if all the water molecules in this volume are replaced by peptide material. At the same time one may also estimate that at most one amino acid residue per three or four lipid molecules interpenetrates the lipid monolayer.

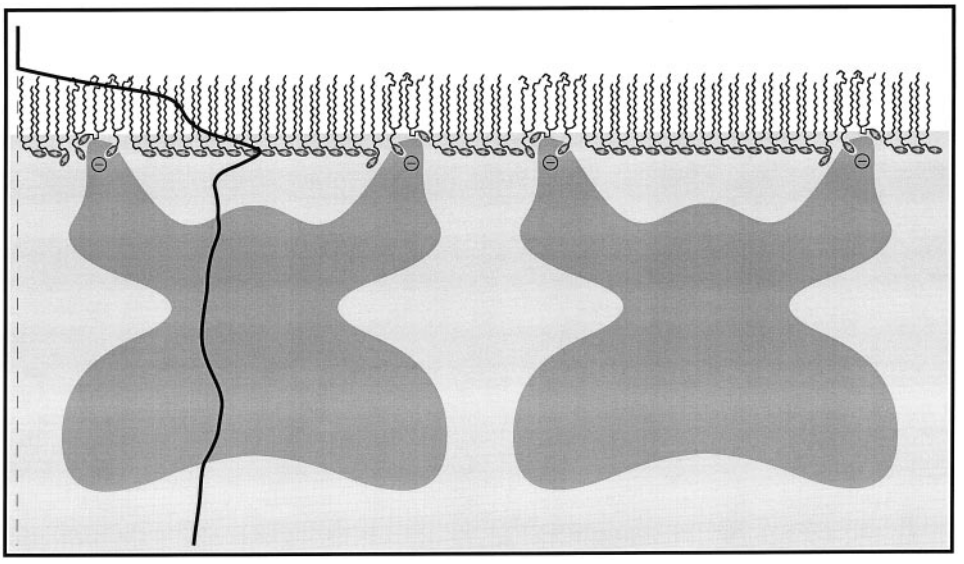

FIGURE 6 Schematic representation of the lipid/protein multilayer structure for S-layer protein from *B. sphaericus* CCM2177 as it emerges from the analysis of the electron density profile (indicated on the left side). Protein and lipids are approximately to scale. There is no structural information for the protein available to date on the atomic scale.

detailed ρ_e profile shown in Fig. 2 *b*. If one assumes that no lipid is removed from the monolayer upon protein binding and crystallization, the electron density profile reflects approximately the distribution of protein and water within the monolayer of protein that constitutes the S-layer. As no detailed 3D structure of the protein is available, the average electron density of the protein has been taken as a reference to estimate the distribution of matter along the surface normal. As the lateral coherence length of the beam in reflectivity experiments is of the order of 1 μm (Vaknin et al., 1991), this distribution is an average over many unit cells. Consequently, water within a cavity or pore in a single protein molecule and water between adjacent protein molecules cannot be discriminated. $\overline{\rho_e} \approx 0.412\ e^-/Å^3$ of the S-layer protein from *B. sphaericus* CCM2177 is estimated from the amino acid contents of the protein given in Table 1 by using tabulated density values of the amino acids (Perkins, 1988) and correcting for the packing of peptide chains in proteins (Lösche et al., 1993). Fig. 7 displays the resulting protein volume fraction profile in which the region close to the lipid monolayer interface reflects the complex topography discussed above. It is directly related to the solid line in Fig. 2 *b* but plotted with the $\hat{z}$ axis vertical (following convention, the ρ_e profiles in Figs. 2 and 5 have been displayed with the z axis pointing along the horizontal). From the plot it is apparent that the S-layer has a thickness of $l_z \approx 90$ Å along the surface normal. This is consistent with available AFM data from which $d \approx 80$ Å has been estimated (Wetzer et al., 1997). The protein forms a cavity (or cavities) within the unit cell that is characterized by two pronounced shoulders of the protein concentration profile at a distance $z \approx -50$ and -105 Å from the surface, where ~60% and 70% of the available area in the horizontal section are attributed to protein, and a pronounced dip at $z \approx -85$ Å where ~80% of the available area is occupied by water. Size exclusion measurements revealed continuous pores of a diameter of $\varnothing \approx 35$ Å in the unit cell of the S-layer (Weigert and Sára, 1996).* The observation that at least 25% of the area within the S-layer is occupied by water at any horizontal section through the layer structure is consistent with this finding. In fact, the x-ray reflectivity result would be consistent with the existence of one large pore ($\varnothing \approx 65$ Å) within the unit cell. The experimental observation of a smaller cutoff diameter of ~35 Å hints at the formation of multiple pores within the unit cell, which could accommodate four pores of this size. Such a structure is in turn consistent with the available EM data (Pum and Sleytr, 1994).

The cleft 3D topography of the S-layer as it appears from the available data is responsible for the structured diffraction pattern observed in GIXD. As shown in Fig. 3, this pattern is consistent with a unit cell size of $(130.5)^2$ Å^2. Integration over the protein volume fraction profile in Fig. 7 yields a total volume of ~760 nm^3 that is occupied by protein within the unit cell. This is only a crude estimate as it does not take into account Ca^{2+} ions that are undoubtedly bound on the protein within the S-layer. From the amino acid composition and the molecular weight $M_r \approx 120{,}000$ for the S-layer protein from *B. sphaericus* CCM2177, it is estimated that one monomeric unit of the S-layer protein should fill a volume V_{prot} of ~155 nm^3. It appears thus most likely that the unit cell in the S-layer is composed of four monomers that form four continuous pores spanning the layer. A more detailed analysis of the diffraction data is in progress.

* In the reference, S-layer proteins from *B. sphaericus* CCM2120 have been investigated. This protein is believed to be very similar to the one from *B. sphaericus* CCM2177. Corresponding measurements with the CCM2177 protein did indeed yield very similar results (M. Sára, personal communication).

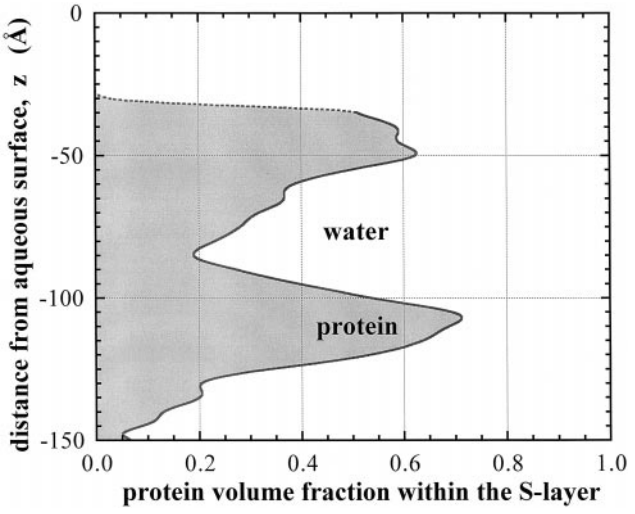

FIGURE 7 Interpretation of the electron density profile of the lipid/protein multilayer structure in terms of the protein (S-layer protein from *B. sphaericus* CCM2177) and water volume fractions within the S-layer at various distances *z* from the aqueous surface. It is clearly seen that the relative proportions of protein and water vary greatly in various horizontal sections within the S-layer.

CONCLUSIONS

Although this study has been concentrating on the S-layer lattice of protein from *B. sphaericus* CCM2177, we believe that the main features of the resulting picture apply in general to S-layers from bacillaceae coupling to lipid membranes. This is due to the strong resemblance of the physicochemical properties of many S-layer proteins studied so far. Moreover, in measurements with different species, e.g., with S-layer protein from *B. coagulans* E38–66, we have observed similar results as those reported here, although the *B. coagulans* protein deviates in physical size and in the detailed structure of its S-layer lattice significantly from the *B. sphaericus* CCM2177 protein.

A detailed picture of the internal structure of S-layers and their coupling to lipid monolayers appears from the analysis of x-ray scattering from layer systems on top of aqueous surfaces. The electrostatic coupling that we have inferred from studies of S-protein adsorption and crystallization at various lipid monolayers (Wetzer et al., 1998) and from a putative partial reorientation of the phospholipid headgroups upon S-layer formation under lipid monolayers is also the most likely coupling mechanism of S-layer proteins to lipid vesicles. The impact of S-layer formation at a lipid interface, if any, is to increase the order on the hydrophobic lipid chains. This has been consistently observed in FTIR spectroscopy (Diederich et al., 1996) and in GIXD (this work). For the S-layer system from *B. sphaericus* CCM2177 attached to DPPE monolayers we have demonstrated in this study that the protein interacts strongly with the PE headgroups. From x-ray reflectometry at high resolution, $Q_z^{max} \approx 0.8$ Å^{-1}, it appears that amino acid side chains or peptide clusters interpenetrate the PE headgroups to a plane in which the phosphates are located and probably further beyond forming close contacts with the glycerol backbones of the lipids. We found compelling evidence that PE headgroups reorient upon protein binding, although it is as yet not clear whether a few headgroups per protein monomer unit in the S-layer reorient by a large angle or all headgroups in the monolayer reorient by a small (average) angle. In terms of the protein structure, the ρ_e profile suggests, consistent with size exclusion measurements with the system (Pum and Sleytr, 1994), that water-filled pores span the S-layer where they form cavities in the center of the S-layer plane.

S-layer-supported lipid films are biomimetic structures observed in cell envelopes of Gram-negative archaebacteria that possess S-layers as the exclusive cell wall component external to the cytoplasmic membrane (Sleytr et al., 1996a). The composite S-layer/lipid system examined in this study involved two selected eubacterial S-layer proteins, that are in vivo attached to a peptidoglycan-containing cell wall layer, and a phospholipid, DPPE, which is not commonly observed in archaebacterial cytoplasmic membranes. However, S-layer attachment to lipid membranes has been shown to increase the film stability of the resulting composite systems significantly. This may lead to the development of novel technologies that exploit these attractive properties, e.g., for the construction of large robust model membranes fit for the investigation of membrane-associated and membrane-integral compounds (Schuster et al., 1998a,b).

We are grateful to F. Rondelez (Institute Curie, Paris, France) for helpful discussions. We thank Jan Skov Pedersen for making available to us his program for form-free fitting of reflectivities (Skov Pedersen and Hamley, 1994) and Jan Skov Pedersen and Michael Gerstenberg for helpful advice. This work has been supported by the German Science Foundation (SFB 294, TP C10), the Austrian Science Foundation (projects S7204/S7205), the BMBF (contract 03-LO4LEI-8), and the Fonds der Chemischen Industrie, Frankfurt, Germany. We acknowledge beam time at HASYLAB (DESY, Hamburg, Germany) and funding by the Danish Dansync program and the EC-TMR program.

REFERENCES

Als-Nielsen, J., D. Jacquemain, K. Kjaer, M. Lahav, F. Leveiller, and L. Leiserowitz. 1994. Principles and applications of grazing incidence x-ray and neutron scattering from ordered molecular monolayers at the air-water interface. *Phys. Rep.* 246:251–313.

Als-Nielsen, J., and K. Kjaer. 1989. X-ray reflectivity and diffraction studies of liquid surfaces and surfactant monolayers. *In* Phase Transitions in Soft Condensed Matter. T. Riste and D. Sherrington, editors. Plenum Press, New York. 113–138.

Als-Nielsen, J., and H. Möhwald. 1991. Synchrotron x-ray scattering studies of Langmuir-films. *In* Handbook on Synchrotron Radiation. S. Ebashi, M. Koch, and E. Rubinstein, editors. Elsevier North-Holland, Amsterdam. 1–53.

Altmann, F. 1992. Determination of amino sugars and amino acids in glycoconjugates using precolumn derivatization with o-phthalaldehyde. *Anal. Biochem.* 204:215–219.

Amos, L. A., R. Henderson, and P. N. T. Unwin. 1982. Three-dimensional structure determination by electron microscopy of two-dimensional crystals. *Prog. Biophys. Mol. Biol.* 39:183–231.

Baumeister, W., and H. Engelhardt. 1987. Three-dimensional structure of bacterial surface layers. *In* Electron Microscopy of Proteins. J. R. Harris and R. W. Horne, editors. Academic Press, London. 109–155.

Beveridge, T. J. 1994. Bacterial S-layers. *Curr. Opin. Struct. Biol.* 4:204–212.

Diederich, A., C. Sponer, D. Pum, U. B. Sleytr, and M. Lösche. 1996. Reciprocal influence between the protein and lipid components of a lipid-protein membrane model. *Colloids Surf. B Biointerf.* 6:335–346.

Hamley, I. W., and J. Skov Pedersen. 1994. Analysis of neutron and x-ray reflectivity data. I. Theory. *J. Appl. Crystallogr.* 27:29–35.

Helm, C. A., H. Möhwald, K. Kjaer, and J. Als-Nielsen. 1987. Phospholipid monolayer density distribution perpendicular to the water surface: a synchrotron x-ray reflectivity study. *Europhys. Lett.* 4:697–703.

Hovmöller, S., A. Sjögren, and D. N. Wang. 1988. The structure of crystalline bacterial surface layers. *Prog. Biophys. Mol. Biol.* 51: 131–163.

Kjaer, K. 1994. Some simple ideas on x-ray reflection and grazing-incidence diffraction from thin surfactant films. *Physica B.* 198: 100–109.

Küpcü, S., M. Sára, and U. B. Sleytr. 1995. Liposomes coated with crystalline bacterial cell surface protein (S-layer) as immobilization structures for macromolecules. *Biochim. Biophys. Acta.* 1235:263–269.

Lösche, M., M. Piepenstock, A. Diederich, T. Grünewald, K. Kjaer, and D. Vaknin. 1993. Influence of surface chemistry on the structural organization of monomolecular protein layers adsorbed to functionalized aqueous interfaces. *Biophys. J.* 65:2160–2177.

Messner, P. 1996. Chemical composition and biosynthesis of S-layers. *In* Crystalline Bacterial Cell Surface Proteins. U. B. Sleytr, P. Messner, D. Pum, and M. Sára, editors. Academic Press, San Diego/Austin. 35–76.

Messner, P., and U. B. Sleytr. 1992. Crystalline bacterial cell-surface layers. *Adv. Microbiol. Physiol.* 33:213–275.

Perkins, S. J. 1988. X-ray and neutron solution scattering. *In* Modern Physical Methods in Biochemistry, Part B. A. Neuberger and L. L. M. V. Deenen, editors. Elsevier, Amsterdam. 143–265.

Pink, D. A., M. Belaya, V. Levadny, and B. Quinn. 1997. A model of polar group statistics in lipid bilayers and monolayers. *Langmuir.* 13: 1701–1711.

Pum, D., M. Sára, and U. B. Sleytr. 1989. Structure, surface charge, and self-assembly of the S-layer lattice from *Bacillus coagulans* E38–66. *J. Bacteriol.* 171:5296–5303.

Pum, D., and U. B. Sleytr. 1994. Large scale reconstitution of crystalline bacterial surface layer (S-layer) proteins at the air/water interface and on lipid films. *Thin Solid Films.* 244:882–886.

Pum, D., and U. B. Sleytr. 1995. Monomolecular reassembly of a crystalline bacterial cell surface layer (S-layer) on untreated and modified Silicon surfaces. *Supramol. Sci.* 2:193–197.

Pum, D., and U. B. Sleytr. 1996. Molecular nanotechnology and biomimetics with S-layers. *In* Crystalline Bacterial Cell Surface Proteins. U. B. Sleytr, P. Messner, D. Pum, and M. Sára, editors. Academic Press/R. G. Landes, San Diego/Austin. 175–209.

Pum, D., G. Stangl, C. Sponer, W. Fallmann, and U. B. Sleytr. 1997. Deep ultraviolet patterning of monolayers of crystalline S-layer protein on Silicon surfaces. *Colloids Surf. B: Biointerf.* 8:157–162.

Pum, D., M. Weinhandl, C. Hödl, and U. B. Sleytr. 1993. Large scale recrystallization of the S-layer of *Bacillus coagulans* E38–66 at the air/water interface and on lipid films. *J. Bacteriol.* 175:2762–2766.

Sára, M., B. Kuen, H. Mayer, F. Mandl, K. C. Schuster, and U. B. Sleytr. 1996. Dynamics in oxygen-induced changes in S-layer protein synthesis from *Bacillus stearothermophilus* PV72 and the S-layer-deficient variant T5 in continuous culture and studies of the cell wall composition. *J. Bacteriol.* 178:2108–2117.

Sára, M., and U. B. Sleytr. 1993. Relevance of charged groups for the integrity of the S-layer from *Bacillus coagulans* E38–66 and for molecular interactions. *J. Bacteriol.* 175:2248–2254.

Sára, M., and U. B. Sleytr. 1996. Crystalline bacterial cell surface layers (S-layers): from cell structure to biomimetics. *Prog. Biophys. Mol. Biol.* 65:83–111.

Schuster, B., D. Pum, O. Braha, H. Bayley, and U. B. Sleytr. 1998a. Self-assembled α-hemolysin pores in an S-layer supported lipid bilayer. *Biochim. Biophys. Acta.* 1370:280–288.

Schuster, B., D. Pum, and U. B. Sleytr. 1998b. Voltage-clamp studies on S-layer supported tetraether lipid membranes. *Biochim. Biophys. Acta.* 1369:51–60.

Skov Pedersen, J., and I. W. Hamley. 1994a. Analysis of neutron and x-ray reflectivity data by constrained least-squares methods. *Physica B.* 198: 16–23.

Skov Pedersen, J., and I. W. Hamley. 1994b. Analysis of neutron and x-ray reflectivity data. II. Constrained least-square methods. *J. Appl. Crystallogr.* 27:36–49.

Sleytr, U. B. 1997. Basic and applied S-layer research: an overview. *FEMS Microbiol. Rev.* 20:5–12.

Sleytr, U. B., P. Messner, D. Pum, and M. Sára (editors). 1996a. Crystalline Bacterial Cell Surface Proteins. Academic Press, San Diego/Austin.

Sleytr, U. B., P. Messner, D. Pum, and M. Sára. 1996b. Occurrence, location, ultrastructure and morphogenesis of S-layers. *In* Crystalline Bacterial Cell Surface Proteins. U. B. Sleytr, P. Messner, D. Pum, and M. Sára, editors. Academic Press, San Diego/Austin. 5–33.

Sleytr, U. B., and M. Sára. 1997. Bacterial and archaeal S-layer proteins: structure-function relationships and their biotechnological applications. *Trends Biotechnol.* 15:20–26.

Sleytr, U. B., M. Sára, S. Küpcü, and P. Messner. 1986. Structural and chemical characterization of S-layers of selected strains of *Bacillus stearothermophilus* and *Desulfotomaculum nigrificans. Arch. Microbiol.* 146:19–24.

Vaknin, D., K. Kjaer, J. Als-Nielsen, and M. Lösche. 1991. Structural properties of phosphatidylcholine in a monolayer at the air/water interface: neutron reflection study and reexamination of x-ray reflection experiments. *Biophys. J.* 59:1325–1332.

Vineyard, G. H. 1982. Grazing-incidence diffraction and the distorted-wave approximation for the study of surfaces. *Phys. Rev. B.* 26:4146.

Weigert, S., and M. Sára. 1996. Ultrafiltration membranes prepared from crystalline bacterial cell surface layers as model systems for studying the influence of surface properties on protein adsorption. *J. Membr. Sci.* 121:185–196.

Weissbuch, I., R. Popovitz-Biro, M. Lahav, L. Leiserowitz, K. Kjaer, and J. Als-Nielsen. 1997. Molecular self assembly into crystals at air-liquid interfaces. *In* Advances in Chemical Physics. I. Prigogine and S. A. Rice, editors. Wiley, New York. 39–120.

Wetzer, B., A. Pfandler, E. Györvary, D. Pum, M. Lösche, and U. B. Sleytr. 1998. S-layer reconstitution at phospholipid monolayers. *Langmuir.* 14:6899–6906.

Wetzer, B., D. Pum, and U. B. Sleytr. 1997. S-layer stabilized solid supported lipid bilayers. *J. Struct. Biol.* 119:123–128.